Analytical Stability Criterion in Haptic Rendering: The Role of Damping

Ahmad Mashayekhi, Saeed Behbahani, Fanny Ficuciello, *Senior Member, IEEE*, and Bruno Siciliano, *Fellow, IEEE*

***Abstract*—A new closed-form equation for stability analysis of a haptic device is presented using frequency response function analysis via continuous time model of the system. Desired impedance of the virtual environment (VE), time delay, and zero-order hold are considered, beside the continuous model of the haptic device. The developed equations provide critical virtual damping and stiffness of the VE versus the mass and viscous friction of the haptic device, sampling time, and time delay. Unlike prior work in this field, the developed equations are valid without any limitation on the values of the time delay and virtual damping. It is shown that they cover available well-known equations in literature for special cases of small values of virtual damping and time delay. The resulting equations are of practical usefulness in many fields, such as surgery simulation for avoiding instability during virtual tool interaction with high-stiffness VEs. The proposed analytical derivation can also be used for studying the effect of operator, sensors, actuator dynamics, and velocity filtering. Simulation and experimental results on the KUKA light weight robot show that the proposed criterion can accurately predict the stability boundaries.**

***Index Terms*—Delay systems, force feedback, haptic interfaces, low pass filters, stability criteria.**

I. Introduction

A HAPTIC device is an interface between a virtual environment (VE) and a human operator for providing the sense of touch when applying the simulated forces/torques by the user [1]. Based on the measured position and velocity of the stylus relative to the virtual object, and the mechanical impedance of the VE, the desired forces/torques are calculated and fed back to the robot. Using the Jacobian matrix of the haptic device, the required forces/torques of the actuators are determined and applied by the actuators. Haptic devices are widely used in applications, such as surgery training for medical students [2], [3], virtual prototyping [4], [5], teleoperation [6], [7], and surgery assistance [8].

The operator's hand has been commonly modeled as mass-spring-damper elements, either the fingers alone [9], or the fingers and wrist [10], or else the whole hand [11]. It has been stated in [12] that the human hand cannot actively add energy to the haptic device at frequencies higher than 10 Hz. Since, instabilities in haptic devices occur at frequencies higher than several hundred hertz, the operator has been considered as a passive element at these frequencies, which only dissipates energy from the system.

In a passive system, the inserted energy to the system is less than the dissipated energy. As a consequence, a passive system is globally stable. On the other hand, the combination of two passive systems is passive too, and therefore stable [13]. Thus, if the operator is omitted in the analysis, the resulted criterion would be conservative. The user dynamics has been involved in the analysis, and its influence makes the system more stable [14], [15]. Colgate has derived his well-known passivity criterion based on this assumption in the absence of the operator [16].

Nonlinear effects, such as Coulomb friction and quantization in the sensors have been studied in [14] and [17]. In [17], the virtual damping has been considered, while the time delay has been overlooked. In [14], the time delay has been considered, while the virtual damping has been ignored. A graphical interpretation of passivity has been proposed in [18] to make the haptic device passive. In this method, the releasing force-position diagram has been set to be always lower than the pressing one while interacting with the VE, with the aim to ensure that no net energy is inserted into the system, and then to make the haptic device behave as a passive system.

Stability of haptic devices has been first studied by Minsky *et al.* [19]. They have used a linear and continuous model for the haptic device and for the VE. Stability analysis in the discrete domain in the absence of the operator has been conducted by Gil *et al.* first without considering time delay [15], and later with taking it into account [20]. They have used a Ruth–Hurwitz and Nyquist approach to derive a linear stability criterion, which is solely valid for small values of B and t_d, as follows [20]:

$$K < \frac{b+B}{\frac{T}{2}+t_d} \tag{1}$$

Manuscript received June 13, 2017; revised September 5, 2017 and December 4, 2017; accepted January 21, 2018. Date of publication January 24, 2018; date of current version April 16, 2018. Recommended by Technical Editor C. Basdogan. This work was supported in part by the FP7 within the RoDyMan project 320992 and in part by the National Grant Multifunctional Smart Hands (MUSHA). *(Corresponding author: Saeed Behbahani.)*

A. Mashayekhi and S. Behbahani are with the Department of Mechanical Engineering, Isfahan University of Technology, Isfahan 84156-83111, Iran (e-mail: a.mashayekhi@me.iut.ac.ir; behbahani@cc.iut.ac.ir).

F. Ficuciello and B. Siciliano are with the CREATE Consortium, PRISMA Laboratory, Department of Electrical Engineering and Information Technology, University of Naples Federico II, Naples 80125, Italy (e-mail: fanny.ficuciello@unina.it; bruno.siciliano@unina.it).

Color versions of one or more of the figures in this paper are available online at http://ieeexplore.ieee.org.

Digital Object Identifier 10.1109/TMECH.2018.2797688

where K, b, B, T, and t_d are the stiffness of virtual wall, the physical damping of the haptic device, the damping of the virtual wall, the sampling time, and the time delay, respectively. They have used a linear model of mass-damper for the haptic device and spring-damper for the VE. Also, the stability boundaries for large values of virtual damping and large time delays have been plotted by solving some complicated equations numerically [20].

Stability boundaries have been found and plotted numerically by considering the influence of the human operator and time delay by Hulin *et al.* [21], [22]. They have also shown that the linear equation derived by Gil *et al.* is valid in the presence of the operator too. Researches show that increasing the physical viscous damping has positive effect on the stability. It can be achieved electrically by adding a resistance in series to a capacitor, totally parallel to the motor [23], or magnetically by adding eddy current brakes [24].

The stability and tracking control problem in the presence of time-varying delay for a bilateral teleoperation has been studied in [25]. A networked teleoperation system with time-varying delay and bounded input has been investigated in [26] for output-feedback based controller design. They have introduced a new fast terminal sliding-mode velocity observer to estimate the unknown velocity signal.

In this paper, a new approach for stability analysis of haptic devices is proposed, leading to a formulation for stability boundaries. For this purpose, the system is analyzed on the boundary of stability in the continuous-time domain (i.e., using Laplace transformation). Since the operator has a positive effect on the stability [12], (s)he is not considered in the current analysis, resulting to a stability criterion for the worst case scenario. Yet, the method presented in this paper can be extended for considering the effect of human operator on the stability.

The proposed formulation gives a stability criterion, which is valid for small and large values of B and t_d. In other words, it removes the main limitation of prior work in this area. Also, it is proved that in the case of small values of B and t_d, this criterion is equivalent to the well-known linear stability equation derived by Gil *et al.* [20]. The developed stability criterion is verified by simulations and experiments.

The paper results can be used to ensure stability in simulated environments, for example in surgical training, where the haptic rendering of rigid surfaces is fulfilled in real time. The stability of the process can be obtained thanks to the possibility of online calculation of the stability boundaries, and consequently changing the system parameters to ensure the stability. Possible examples of application of the proposed stability criterion include simulation of needle insertion through variable stiffness layers for epidural lumbar puncture, spine biopsy, and neurosurgical probe insertion [27].

In the next section, the system description and model of the haptic device are presented. The proposed stability analysis and the developed stability criterion are presented in Section III. In Section IV, it is shown that the presented stability criterion is consistent with the special case of the linear stability criterion presented by Gil. *et al.* [20]. In addition, in the case of large delay, the stability criterion is reduced to a simple and accurate stability equation. For validating the stability criterion, simulations and experiments are elaborated in Sections V and VI, respectively. The effect of a velocity filter is discussed in the succeeding section.

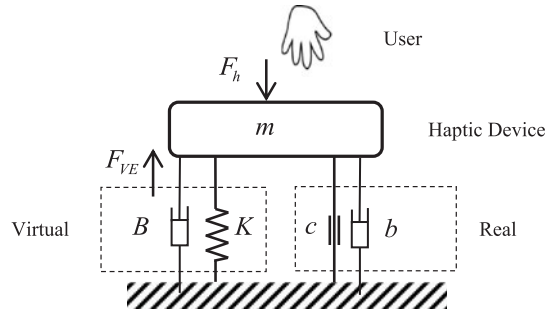

Fig. 1. Schematic view of a 1-DOF haptic device.

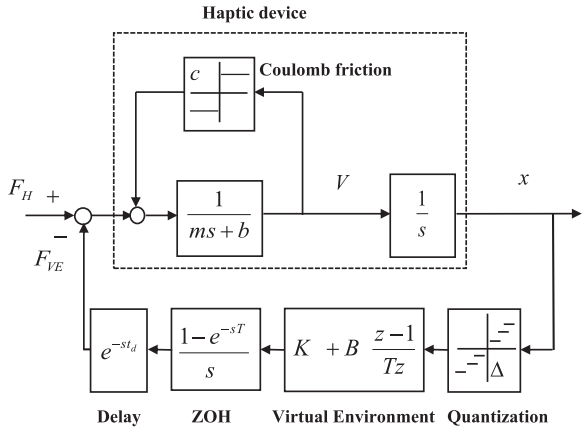

Fig. 2. Nonlinear model of the haptic device.

II. System Description

A schematic view of a 1-degree of freedom (1-DOF) haptic device is presented in Fig. 1. The mass of the robot is denoted by m, whereas the Coulomb and viscous coefficients of friction are denoted by c and b, respectively. F_{VE} is the applied force by the controller that simulates the virtual wall for the user, with the stiffness of K and damping of B. A nonlinear model of the haptic device is depicted in Fig. 2. The continuous position of the end-effector of the haptic device (x) is measured by a sensor with effective resolution of Δ. It is assumed that there is no velocity sensor; therefore, the backward difference is used to determine the velocity, without any filter. The robot links are assumed to be rigid, without any internal vibration. Also, the actuators are assumed to be continuous with no saturation. The force of the VE (F_{VE}), which is supposed to be applied on the operator's hand by the haptic device, is fed back to the system after being held in a zero-order hold (ZOH), and after a time delay equal to t_d. This delay can be the sum of computation, communication, and sensor delays. The difference between the exerted force of the operator's hand and the calculated reaction force from the VE is the total force on the haptic device that accelerates the stylus.

In [14] and [17], it has been shown that the maximum generated energy in the sensors due to quantization is less than the minimum dissipated energy due to Coulomb friction in all

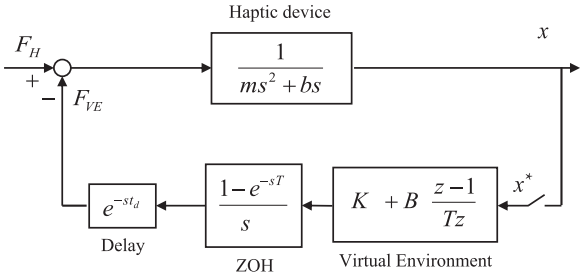

Fig. 3. Linear model of the haptic device.

TABLE I
DIMENSIONLESS PARAMETERS

Parameter	Variable	Dimensionless variable
Sampling time	T	–
Mass	m	–
Delay	t_d	$d = t_d/T$
Virtual stiffness	K	$\alpha = KT^2/m$
Virtual damping	B	$\beta = BT/m$
Physical damping	b	$\delta = bT/m$

commercial and famous haptic devices. Also, a more precise analysis has shown that these two nonlinear effects could be omitted in the stability analysis [28] and leading to a linear and simpler model for the haptic device as shown in Fig. 3.

For reducing the number of total effective parameters in stability analysis, the dimensionless parameters presented in Table I are utilized in this paper, which are similar to the parameters used in [21].

III. NOVEL STABILITY CRITERION

A new straightforward stability criterion is developed in this section, which can eventually be presented as a closed-form equation. A simplified model of the haptic device is illustrated in Fig. 3. In this figure, the VE is modeled as a discrete PD controller. The only discrete part of this model is the VE, which should be converted to its continuous-time equivalent. The term $B\frac{z-1}{Tz}x^*$ can be rewritten as $B\frac{z-1}{Tz}x^* \cong Z\left[B\frac{x(k)-x(k-1)}{T}\right]$. It means that B is multiplied by the average velocity of current and previous samples. In other words, in the discrete model, B is multiplied by the instant velocity of half of sampling time before. Therefore, the equivalent continuous model should also use the velocity with a delay of $T/2$. Then, the equivalent continuous model for this term would be $Bse^{-sT/2}$. The equivalent continuous model of the haptic device is depicted in Fig. 4. From Fig. 4, the transfer function of the closed-loop system $G(s)$ can be easily calculated and simplified as follows:

$$G(s) = \frac{sT}{d(s)} \tag{2}$$

where $d(s)$ is the characteristic equation of the transfer function as

$$\begin{aligned} d(s) = &\left(ms^2 + bs\right) sT \\ &+ e^{-st_d}\left(1 - e^{-sT}\right)\left(K + Bse^{-sT/2}\right). \end{aligned} \tag{3}$$

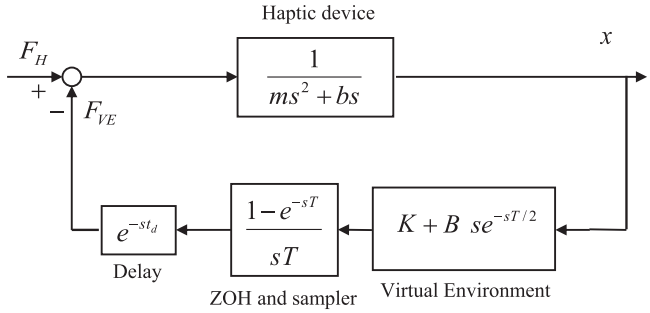

Fig. 4. Continuous model of a haptic device.

When the system is on the stability boundary, the characteristic equation has roots located on the imaginary axis, which means that $s = j\omega$ would satisfy the characteristic equation. Note that ω is the frequency and starts from zero. By substituting $e^{j\alpha\omega} = \cos(\alpha\omega) + j\sin(\alpha\omega)$, the characteristic equation becomes

$$\begin{aligned} &\left(m(j\omega)^2 + b(j\omega)\right)(j\omega)T \\ &+ \left(\cos(t_d\,\omega) - j\sin(t_d\,\omega)\right) \times \left(1 - \cos(T\omega) + j\sin(T\omega)\right) \\ &\quad \times \left(K + B(j\omega)\left(\cos(T\omega/2) - j\sin(T\omega/2)\right)\right) = 0. \end{aligned} \tag{4}$$

After simplification, the characteristic equation will be

$$\begin{aligned} &\left[K\sin((T+t_d)\omega) - K\sin(t_d\omega) - B\omega\cos((3T/2+t_d)\omega)\right. \\ &\quad \left. + B\omega\cos((T/2+t_d)\omega) - Tm\omega^3\right] j \\ &+ \left(K\cos(t_d\omega) - K\cos((T+t_d)\omega) - B\omega\sin((3T/2+t_d)\omega)\right. \\ &\quad \left. + B\omega\sin((T/2+t_d)\omega) - Tb\omega^2\right) = 0. \end{aligned} \tag{5}$$

If this equation holds, then the real and imaginary parts of the left-hand side of the equation should be equal to zero. Consequently, two independent equations are obtained, that can be solved for K and B and then simplified as

$$\begin{cases} K = T\omega^2 \times \dfrac{m\omega\cos((T+t_d)\omega) + b\sin((T+t_d)\omega)}{\sin(T\omega)} \\ B = T\omega \times \dfrac{m\omega\sin((T/2+t_d)\omega) - b\cos((T/2+t_d)\omega)}{\sin(T\omega)}. \end{cases} \tag{6}$$

By using the dimensionless parameters in Table I and defining a new dimensionless parameter $\phi = \omega T$, the above-mentioned equations can be rewritten as follows:

$$\begin{cases} \alpha = \phi^2 \times \dfrac{\phi\cos((d+1)\phi) + \delta\sin((d+1)\phi)}{\sin(\phi)} \\ \beta = \phi \times \dfrac{\phi\sin((d+0.5)\phi) - \delta\cos((d+0.5)\phi)}{\sin(\phi)}. \end{cases} \tag{7}$$

Fig. 5 shows the dimensionless stiffness of virtual wall (α) plotted versus the dimensionless damping of the virtual wall (β) for delays of $d = [0, 1, 2]$. From Fig. 5, it is clear that the higher the time delay, the lower the maximum achievable stiffness of the virtual wall. The maximum achievable stiffness and the maximum achievable virtual damping are shown with circle and triangle markers, respectively.

Hulin and Gil have determined linear stability boundaries only for small values of B and t_d in [20], [21], whereas the

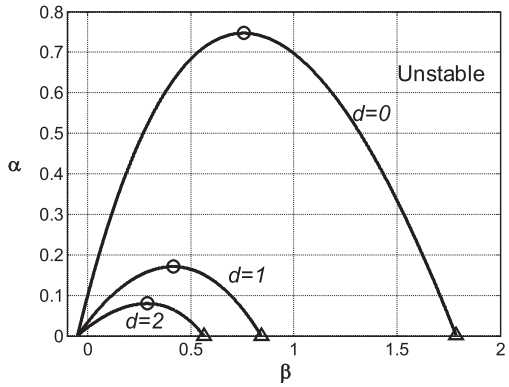

Fig. 5. Dimensionless stiffness versus dimensionless virtual damping.

developed stability criterion in this paper does not have any restriction or limitation on these parameters. In addition, in prior work the stability boundary has to be plotted numerically, by solving complicated equations, whereas in the developed criterion, they are determined more quickly, using the closed-form equations (6) or (7). It has to be mentioned that having closed-form equations for fast determination of stability boundaries is of crucial importance in real-time applications.

From (6) and (7), it is clear that the following equations are valid:

$$\begin{cases} \lim K_{\omega\to 0} = 0 & \text{and} \quad \lim B_{\omega\to 0} = -b \\ \lim \alpha_{\phi\to 0} = 0 & \text{and} \quad \lim \beta_{\phi\to 0} = -\delta \end{cases} \tag{8}$$

which means that in the diagram of K versus B (or α versus β), the starting point is $(K, B) = (0, -b)$ (or $(\alpha, \beta) = (0, -\delta)$) that is also consistent with the results of prior work [20], [21].

In (6), the value of ω should be varied from zero to a certain value of $\omega_{\max}$. When $\omega = 0$, it can be concluded that $(K, B) = (0, -b)$. When $\omega = \omega_{\max}$, the points shown by triangle marks in Fig. 5 are obtained. For the first time, the following equation is derived in this paper for calculating $\omega_{\max}$ (see Appendix A):

$$\omega_{\max} = \frac{1}{T + t_d} \times \frac{-(p_2 - aq_1) - \sqrt{(p_2 - aq_1)^2 - 4p_3(p_1 - a)}}{2(p_1 - a)} \tag{9}$$

where in this equation $a = m/b(T + t_d)$ and $p_1 = -0.4087$, $p_2 = 1.325$, $p_3 = 0.07507$, and $q_1 = -\pi/2$.

IV. Special Case

Equation (6) has been derived without any restriction on the values of the time delay or the virtual damping. There are two special cases that are worth to be analyzed, respectively, with the aim to derive special formulations for them.

A. Small Virtual Damping

As discussed in the reviewed literature, for small values of B, a linear relation between K and B has been suggested (1). In this section, for validating the proposed framework, this linear equation is obtained from (6) for small values of ω. Small values of ω lead to small vales of $(T + t_d)\omega$ too. Using this assumption, (6) will be simplified as follows:

$$\begin{aligned} K &= T\omega^2 \times \frac{m\omega\cos((T + t_d)\omega) + b\sin((T + t_d)\omega)}{\sin(T\omega)} \\ &= T\omega^2 \times \frac{m\omega + b(T + t_d)\omega}{t\omega} \\ &= (m + b(T + t_d))\omega^2 \end{aligned} \tag{10}$$

and

$$\begin{aligned} B &= T\omega \times \frac{m\omega\sin((T/2 + t_d))\omega - b\cos((T/2 + t_d)\omega)}{\sin(T\omega)} \\ &= t\omega \times \frac{m\omega^2(T/2 + t_d) - b}{T\omega} \\ &= m\omega^2(T/2 + t_d) - b. \end{aligned} \tag{11}$$

Omitting ω in (10) and (11) leads to the following equation:

$$K = (B + b) \times \frac{b(T + t_d) + m}{m(T/2 + t_d)}. \tag{12}$$

The above equation can be simplified as

$$\begin{aligned} K &= (B + b) \times \left[\frac{b}{m}\frac{T + t_d}{T/2 + t_d} + \frac{1}{T/2 + t_d}\right] \\ &= (B + b) \times \left[\left(\frac{bT}{m}\right)\frac{1 + t_d/T}{T/2 + t_d} + \frac{1}{T/2 + t_d}\right]. \end{aligned} \tag{13}$$

From the definition of $\delta = bT/m$ and knowing that $\delta < 0.02$ [21], the first term in the above equation can be omitted, leading to the following equation:

$$K = \frac{b + B}{\frac{T}{2} + t_d}. \tag{14}$$

Equation (14) is identical to the linear introduced in Section I, which shows that the general criterion developed in this paper is consistent with the well-established linear stability equation for small values of B and t_d.

B. Large Time Delay

In some applications, time delays are significantly large due to different sources, such as computation (e.g., haptic rendering of deformable objects modeled by finite-element) or communication (e.g., network controlled systems). In this case, the sampling time T is negligible when compared with the time delay t_d. Then (6) can be simplified, and K and B can be calculated as follows:

$$\begin{cases} K = m\omega^2\cos(t_d\omega) + b\omega\sin(t_d\omega) \\ B = m\omega\sin(t_d\omega) - b\cos(t_d\omega). \end{cases} \tag{15}$$

This equation is suitable to predict a stability boundary for large time delays (i.e., $d = t_d/T > 50$) for both small and large amounts of B. This equation is verified by simulations and experiments in the next sections. From Fig. 5, it is clear that the stability boundary has a peak point. It means that there is a specified value for β, which leads to the maximum value of α (i.e., circle marks in Fig. 5). Determining this special

value of β and its corresponding α is useful in many applications. In applications where the time delay is much larger than the sampling time, the maximum achievable value of K would be low. To provide a VE with the highest achievable stiffness, one could choose this specified value for B to achieve the maximum K.

The value of ω that leads to the maximum value of K is determined from the following equation (see Appendix B):

$$\omega^{K_{\max}} = \frac{\frac{\pi}{2}(A^*) + \sqrt{\left(\frac{\pi}{2}A^*\right)^2 + 4bt_d(A^* + m)}}{2(A^* + m)t_d} \tag{16}$$

where $A^* = 2m + bt_d$. Substituting $\omega = \omega^{K_{\max}}$ in (6) leads to the operating points with the maximum stiffness of the VE (i.e., circle markers in Fig. 5).

Equation (6) facilitates the parameter study on the effect of variation of each parameter on the boundary of stability. For example, in the case of multi-DOF haptic device, the effective mass and viscous friction of the system depend on the instantaneous configuration of the system. Using either online or offline parameter estimation with lookup tables, the real values of inertia and viscous friction can be substituted in (6) and the stability boundary can be readily computed.

V. Simulation Results

A Simulink model in MATLAB software has been created based on the block diagram of Fig. 3. However, a ZOH block has been used in lieu of its equivalent Laplace model. For each B, the allowable K can be found by gradually increasing K until unstable response is observed. The stability boundaries can then be computed by repeating the simulation many times and for different values of B. In the following subsections, the stability boundaries obtained from the time-consuming simulation are compared with the boundaries found from the developed criteria. For comparison, the dimensionless virtual stiffness (α) is plotted versus dimensionless virtual damping (β).

A. General Case

To verify (6) and (7), which have been derived for the general case of the problem (i.e., regardless the value of virtual damping and time delay), two values for delay, $d = [0, 1]$ have been chosen. A comparison between the analytical and simulation results is shown in Fig. 6. From Fig. 6, it is clear that the stability formula can predict stability boundaries with good precision. In the case of no delay (i.e. $d = 0$), there is a difference between the results of stability equations and simulations. In fact, the stability equations are a little more conservative if compared with the simulation results. This error is rather considerable for very large values of β and for situations where the peak point of α is passed. In most practical applications, the working point is chosen near or before the peak point of α. Therefore, the developed formulas can be utilized appropriately in practical applications. For larger delays (i.e. $d > 1$) there is no error between simulation and formula.

B. Large Time Delay

In this subsection, the validity of (15) is investigated, which has been derived for large time delays. The value of $\delta = 0.02$

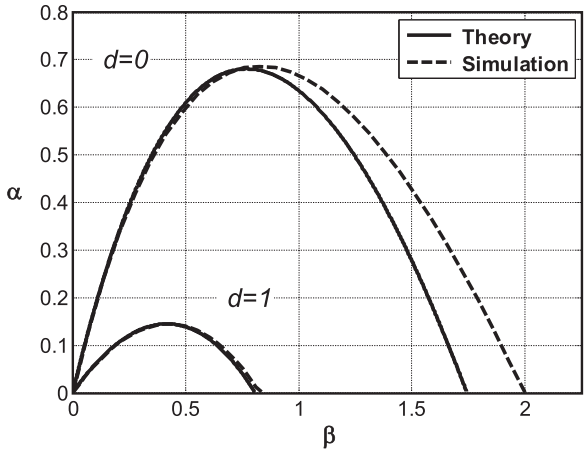

Fig. 6. Stability boundary in $\beta - \alpha$ plane for $d = [0, 1]$. Solid lines are plotted using (7) and dashed lines are plotted from simulation results. In the case of $d = 1$, both graphs are actually the same.

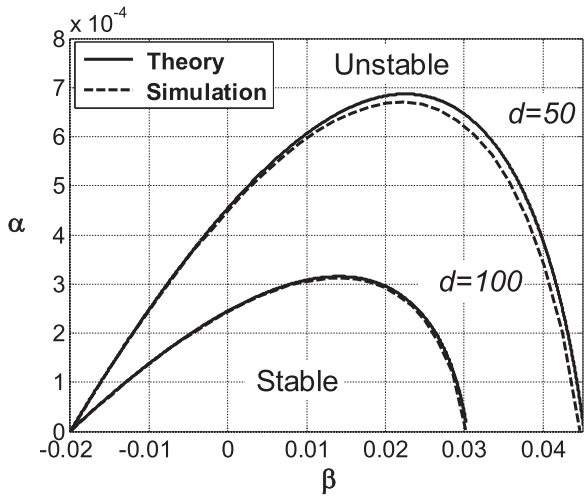

Fig. 7. Theoretical stability boundary (solid line) and simulation results (dash line) for large amount of delay.

and delays of $d = [50, 100]$ have been chosen and analyzed. Fig. 7 compares the results obtained from the developed stability criterion with the simulation results. From this figure, it is clear that (15) is suitable for prediction of the stability boundary in the case of very large delays (i.e., $d \geq 50$) for both small and large values of β. It should be mentioned that the small difference between theory and simulation in Fig. 7 in the case of $d = 50$ can be resolved by using (7).

VI. Experiments

The first axis of the KUKA light weight robot (LWR) (see Fig. 8) has been utilized for experimental investigation and verification of the proposed theories. This robot has been widely used in impedance control applications [29]. Each joint has an impedance controller that is able to compensate gravity and Coulomb friction. Due to high resolution of position sensors, the nonlinear effects of quantization are negligible.

A bilateral virtual wall consisting of a virtual damping and virtual spring is simulated as VE. For a known value of virtual damping, the value of virtual spring is changed and the stability

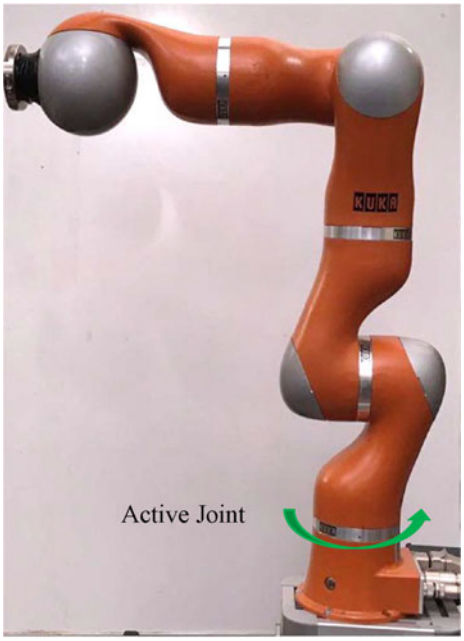

Fig. 8. KUKA LWR as the experimental device.

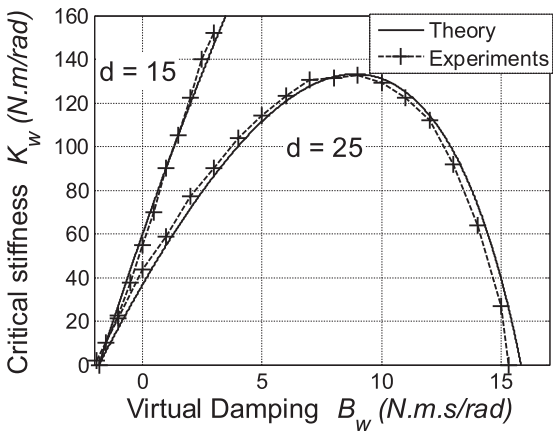

Fig. 9. Experimental and theoretical stability boundary for delays of 30 and 50 ms.

of the haptic system is checked. The amplitude of stable oscillations converges to zero, while for unstable oscillations the amplitude obviously diverges.

As reported in the FRI library [30], the moment of inertia of the robot arm around its axis of rotation is 0.4848 kg·m^2. The sampling time has been set to 2 ms and significant delays of 30 and 50 ms have been added to the control loop artificially (i.e., $d = 15$ and $d = 25$). Theoretical and experimental stability boundaries have been compared in Fig. 9, which shows a good agreement between them.

VII. Velocity Filtering

In the presented stability analysis, it is assumed that no velocity sensor exists, and the simple backward difference is used to calculate the velocity without any filtering. This assumption is

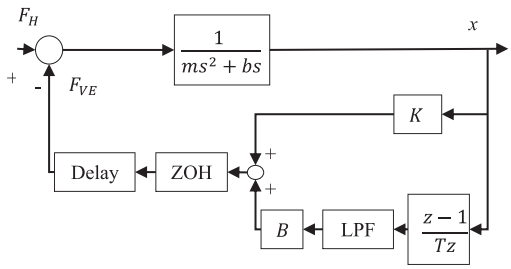

Fig. 10. Continuous model of a linear haptic system, with velocity filter.

widely used in the literature [15], [20], [21]. In the experiments, due to the high resolution of the position sensor and a sampling rate of 500 Hz, there has been no need for low-pass filter (LPF). In some applications a velocity filter is needed, for example due to low resolution or a fast sampling rate. The developed method can be used to analyze the linear haptic device with/without velocity filter, or any other signal processing. For this purpose, the Laplace model of the signal processing (e.g., velocity filter) is placed in the control loop, such as in Fig. 10.

As an example, a first-order LPF with cutoff frequency of ω_c is considered as a velocity filter, and the effect of ω_c on the stability boundaries is discussed. This LPF has the following Laplace model:

$$G_{\text{Lpf}}(s) = \frac{\omega_c}{s+\omega_c} = \frac{1}{s/\omega_c + 1}. \tag{17}$$

By simplifying the closed-loop model depicted in Fig. 10, and following the procedure described in Section III, the characteristic equation of the system is (after substituting $s = j\omega$ for determining the boundary of stability)

$$\begin{aligned} &\left(m(j\omega)^2 + b(j\omega)\right)\left(1+\frac{j\omega}{w_c}\right)(j\omega)T \\ &+ \left(\cos\left(t_d\omega\right) - j\sin\left(t_d\omega\right)\right) \\ &\times \left(1-\cos\left(T\omega\right) + j\sin\left(T\omega\right)\right) \\ &\times \left(K\left(1+\frac{j\omega}{w_c}\right) + B(j\omega)\left(\cos\left(\omega T/2\right) - j\sin\left(\omega T/2\right)\right)\right) = 0. \end{aligned} \tag{18}$$

Like above, if (18) holds, then the real and imaginary parts of (18) should be equal to zero. Then, there are two independent equations, that should be solved for K and B. The resulting equations are more complicated than (6). For any value of ω_c, stability boundaries can easily be plotted by gradually increasing ω. In Fig. 11, the dimensionless virtual damping versus the dimensionless virtual stiffness has been plotted for different values of ω_c and the obtained boundaries have been compared with the case of not using a filter. It is clear that using a first-order LPF destabilizes the system, due to its inherent delay. Other types of velocity filters can be similarly analyzed. In fact, any other linear transfer function coming from the sensor transfer function, electrical drive, actuator dynamics, amplifier, or signal processing can be accommodated in the control loop and its effect on the stability can be studied accordingly.

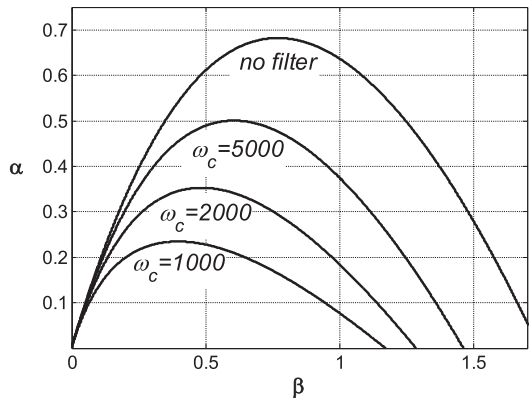

Fig. 11. Stability boundaries for different values of cutoff frequency.

VIII. Conclusion

A new criterion has been developed for the stability analysis of haptic devices, without any restriction or limitation on time delay and virtual damping, in the absence of the operator. This stability criterion is a closed-form formulation between the effective mass and physical viscous friction of the haptic device, sampling time, time delay, virtual stiffness, and virtual damping of the environment. Any other dynamic effect (e.g., operator, velocity filter, signal processing, sensor, and actuator dynamics) can be accommodated in the developed framework, as long as it is linear. The criterion has been customized for some special and practical applications, including low virtual damping and large time delay. The developed formulas have been verified by simulations as well as by experiments on a KUKA LWR.

Using the method presented in this paper, the effect of velocity filter on the stability can be studied. As an example, a first-order LPF has been considered and the effect of its cutoff frequency on the stability has been analyzed, which has shown that increasing the cutoff frequency leads to raising the stability boundary.

Appendices

Appendix A (Maximum Permissible Values of ω)

The maximum value of ω corresponds to the triangle markers in Fig. 5, where $K = 0$. From (6) we have

$$K = T\omega^2 \times \frac{m\omega \cos\left((T+t_d)\omega\right) + b \sin\left((T+t_d)\omega\right)}{\sin\left(T\omega\right)} = 0. \tag{19}$$

The above-mentioned equation is valid in two points. The first point is the obvious point of $\omega = 0$, which is the point in Fig. 5 with $K = 0$ and $B = -b$. The second point corresponds to the maximum value of B (i.e., triangle points in Fig. 5). At these points the following equation holds:

$$m\omega \cos\left((T+t_d)\omega\right) + b \sin\left((T+t_d)\omega\right) = 0. \tag{20}$$

After simplification, by defining a new parameter as $X = (T+t_d)\,\omega \geq 0$, the following equation is obtained:

$$\frac{m}{b(T+t_d)} X = -\tan\left(X\right). \tag{21}$$

The left-hand side of this equation is a line with positive slope of $m/\left(b\left(T+t_d\right)\right)$. It is clear that the solution to (21) is in the interval of $X \in (\pi/2, \pi)$. Using curve fitting toolbox, a good approximation for $-\tan\left(X\right)$ is the following equation:

$$-\tan\left(X\right) \cong \frac{p_1 X^2 + p_2 X + p_3}{X + q_1} \quad \text{for } X \in (\pi/2, \pi) \tag{22}$$

where $p_1 = -0.4087, p_2 = 1.325, p_3 = -0.07507$, and $q_1 = -\pi/2$. Substituting (22) into (21) leads to

$$\frac{p_1 X^2 + p_2 X + p_3}{X + q_1} = \frac{m}{b(T+t_d)} X. \tag{23}$$

Defining $a = m/(b(T+t_d))$ and solving (23) for X, the following equation is obtained:

$$X = \frac{(p_2 - aq_1) + \sqrt{(p_2 - aq_1)^2 - 4p_3(p_1 - a)}}{2(a - p_1)}. \tag{24}$$

Using the definition of X, it can be concluded that

$$\omega_{\max} = \frac{1}{T+t_d} \times \frac{(p_2 - aq_1) + \sqrt{\left(p_2 - aq_1\right)^2 - 4p_3\left(p_1 - a\right)}}{2(a - p_1)}. \tag{25}$$

Appendix B (Determination of Maximum Stiffness of Virtual Wall)

From (15), in the case of large time delay, K is as follows:

$$K = m\omega^2 \cos\left(t_d\omega\right) + b\omega \sin\left(t_d\omega\right). \tag{26}$$

At the point where K is maximum, we have

$$\frac{dK}{d\omega} = 0. \tag{27}$$

After simplification and defining a new parameter as $X = \omega t_d$, the following equation is obtained:

$$\tan\left(X\right) = \frac{(2m + bt_d)X}{mX^2 - bt_d}. \tag{28}$$

A good approximation for $\tan\left(x\right)$ in the interval of $X \in (0, \pi/2)$ is $1/(x - \pi/2)$. After some simplifications, X is determined as

$$X = \frac{\frac{\pi}{2}\left(A^*\right) + \sqrt{\left(\frac{\pi}{2}A^*\right)^2 + 4bt_d(A^* + m)}}{2(A^* + m)} \tag{29}$$

where $A^* = 2m + bt_d$. Using the definition of X, ω is determined as follows:

$$\omega^{K_{\max}} = \frac{\frac{\pi}{2}\left(A^*\right) + \sqrt{\left(\frac{\pi}{2}A^*\right)^2 + 4bt_d(A^* + m)}}{2(A^* + m)t_d}. \tag{30}$$

The value of ω that is calculated from the above-mentioned equation leads to the maximum value of virtual stiffness of the VE in the case of large delay (i.e., circle markers in Fig. 5).

References

[1] B. Siciliano and O. Khatib, *Springer Handbook of Robotics*, 2nd ed. New York, NY, USA: Springer-Verlag, 2016.

[2] C. Basdogan, S. De, J. Kim, M. Muniyandi, H. Kim, and M. A. Srinivasan, "Haptics in minimally invasive surgical simulation and training," *IEEE Comput. Graph. Appl.*, vol. 24, no. 2, pp. 56–64, Mar./Apr. 2004.

[3] A. Mashayekhi, A. Nahvi, M. Yazdani, M. Mohammadi Moghadam, M. Arbabtafti, and M. Norouzi, "Virsense: A novel haptic device with fixed-base motors and a gravity compensation system," *Ind. Robot, Int. J.*, vol. 41, no. 1, pp. 37–49, 2014.
[4] E. Chen, "Six degree-of-freedom haptic system for desktop virtual prototyping applications," in *Proc. 1st Int. Workshop Virtual Reality Prototyping*, 1999, pp. 97–106.
[5] W. Zhu and Y.-S. Lee, "Five-axis pencil-cut planning and virtual prototyping with 5-dof haptic interface," *Comput.-Aided Design*, vol. 36, no. 13, pp. 1295–1307, 2004.
[6] X. Yin, S. Guo, N. Xiao, T. Tamiya, H. Hirata, and H. Ishihara, "Safety operation consciousness realization of a mr fluids-based novel haptic interface for teleoperated catheter minimally invasive neurosurgery," *IEEE/ASME Trans. Mechatronics*, vol. 21, no. 2, pp. 1043–1054, Apr. 2016.
[7] Z. T. H. Tse, H. Elhawary, M. Rea, B. Davies, I. Young, and M. Lamperth, "Haptic needle unit for mr-guided biopsy and its control," *IEEE/ASME Trans. Mechatronics*, vol. 17, no. 1, pp. 183–187, Feb. 2012.
[8] F. Fazioli, F. Ficuciello, G. Fontanelli, B. Siciliano, and L. Villani, "Implementation of a soft-rigid collision detection algorithm in an open-source engine for surgical realistic simulation," in *Proc. 2016 IEEE Int. Conf. Robot. Biomimetics*, 2016, pp. 2204–2208.
[9] R. B. Gillespie and M. R. Cutkosky, "Stable user-specific haptic rendering of the virtual wall," in *Proc. ASME Int. Mech. Eng. Congr. Exhib.*, 1996, vol. 58, pp. 397–406.
[10] R. G. Dong, J. H. Dong, J. Z. Wu, and S. Rakheja, "Modeling of biodynamic responses distributed at the fingers and the palm of the human hand–arm system," *J. Biomech.*, vol. 40, no. 10, pp. 2335–2340, 2007.
[11] T. Yoshikawa and Y. Ichinoo, "Impedance identification of human fingers using virtual task environment," in *Proc. 2003 IEEE/RSJ Int. Conf. Intell. Robots Syst.*, 2003, vol. 4, pp. 3094–3099.
[12] N. Hogan, "Controlling impedance at the man/machine interface," in *Proc. 1989 IEEE Int. Conf. Robot. Autom.*, 1989, pp. 1626–1631.
[13] A. van der Schaft, *L2-Gain and Passivity Techniques in Nonlinear Control*. New York, NY, USA: Springer-Verlag, 2017.
[14] N. Diolaiti, G. Niemeyer, F. Barbagli, and J. K. Salisbury, "Stability of haptic rendering: Discretization, quantization, time delay, and coulomb effects," *IEEE Trans. Robot.*, vol. 22, no. 2, pp. 256–268, Apr. 2006.
[15] J. J. Gil, A. Avello, A. Rubio, and J. Florez, "Stability analysis of a 1 dof haptic interface using the routh-hurwitz criterion," *IEEE Trans. Control Syst. Technol.*, vol. 12, no. 4, pp. 583–588, Jul. 2004.
[16] J. E. Colgate and G. Schenkel, "Passivity of a class of sampled-data systems: Application to haptic interfaces," in *Proc. 1994 Amer. Control Conf.*, 1994, vol. 3, pp. 3236–3240.
[17] J. J. Abbott and A. M. Okamura, "Effects of position quantization and sampling rate on virtual-wall passivity," *IEEE Trans. Robot.*, vol. 21, no. 5, pp. 952–964, Oct. 2005.
[18] J.-H. Ryu and M.-Y. Yoon, "Memory-based passivation approach for stable haptic interaction," *IEEE/ASME Trans. Mechatronics*, vol. 19, no. 4, pp. 1424–1435, Aug. 2014.
[19] M. Minsky, O.-y. Ming, O. Steele, F. P. Brooks Jr., and M. Behensky, "Feeling and seeing: issues in force display," in *Proc. ACM SIGGRAPH Comput. Graph.*, 1990, vol. 24, pp. 235–241.
[20] J. J. Gil, E. Sánchez, T. Hulin, C. Preusche, and G. Hirzinger, "Stability boundary for haptic rendering: Influence of damping and delay," *J. Comput. Inf. Sci. Eng.*, vol. 9, no. 1, 2009, Art. no. 011005.
[21] T. Hulin, A. Albu-Schaffer, and G. Hirzinger, "Passivity and stability boundaries for haptic systems with time delay," *IEEE Trans. Control Syst. Technol.*, vol. 22, no. 4, pp. 1297–1309, Jul. 2014.
[22] T. Hulin, C. Preusche, and G. Hirzinger, "Stability boundary for haptic rendering: Influence of human operator," in *Proc. IEEE/RSJ Int. Conf. Intell. Robots Syst.*, 2008, pp. 3483–3488.
[23] J. S. Mehling, J. E. Colgate, and M. A. Peshkin, "Increasing the impedance range of a haptic display by adding electrical damping," in *Proc. 1st Joint 2005 Eurohaptics Conf., Symp. Haptic Interfaces Virtual Environ. Teleoperator Syst., World Haptics*, 2005, pp. 257–262.
[24] A. H. Gosline, G. Campion, and V. Hayward, "On the use of eddy current brakes as tunable, fast turn-on viscous dampers for haptic rendering," in *Proc. Eurohaptics*, 2006, pp. 229–234.
[25] S. Islam, P. Liu, A. El Saddik, and Y. B. Yang, "Bilateral control of teleoperation systems with time delay," *IEEE/ASME Trans. Mechatronics*, vol. 20, no. 1, pp. 1–12, Feb. 2015.
[26] C. Hua, Y. Yang, and P. X. Liu, "Output-feedback adaptive control of networked teleoperation system with time-varying delay and bounded inputs," *IEEE/ASME Trans. Mechatronics*, vol. 20, no. 5, pp. 2009–2020, Oct. 2015.
[27] S. P. DiMaio and S. E. Salcudean, "Interactive simulation of needle insertion models," *IEEE Trans. Biomed. Eng.*, vol. 52, no. 7, pp. 1167–1179, Jul. 2005.
[28] A. Mashayekhi, R. B. Boozarjomehry, A. Nahvi, A. Meghdari, and P. Asgari, "Improved passivity criterion in haptic rendering: influence of coulomb and viscous friction," *Adv. Robot.*, vol. 28, no. 10, pp. 695–706, 2014.
[29] F. Ficuciello, L. Villani, and B. Siciliano, "Variable impedance control of redundant manipulators for intuitive human–robot physical interaction," *IEEE Trans. Robot.*, vol. 31, no. 4, pp. 850–863, Aug. 2015.
[30] G. Schreiber, A. Stemmer, and R. Bischoff, "The fast research interface for the kuka lightweight robot," in *Proc. 2010 IEEE Int. Conf. Robot. Autom., Workshop Innov. Robot Control Arch. Demanding (Res.) Appl. How Modify Enhance Commercial Controllers*, 2010, pp. 15–21.

Ahmad Mashayekhi received the B.Sc. degree in mechanical engineering from the K. N. Toosi University of Technology, Tehran, Iran, in 2008 and the M.Sc. degree in mechatronics engineering from Sharif University of Technology, Tehran, Iran, in 2011. He is currently working toward the Ph.D. degree in mechanical engineering from Isfahan University of Technology, Isfahan, Iran.

From November 2016 to July 2017, he was a visiting scholar with the PRISMA Lab, University of Naples Federico II, Naples, Italy. His current research interests include mechatronics, robotics, and haptics.

Mr. Mashayekhi was the recipient of a bronze medal in Physics Olympiad in 2002.

Saeed Behbahani received the B.Sc. and M.Sc. degrees in mechanical engineering from the Mechanical Engineering Department, Amir Kabir University of Technology, Tehran, Iran, in 1996 and 1998, respectively, and the Ph.D. degree in mechanical engineering from the Mechanical Engineering Department, University of British Columbia, Vancouver, BC, Canada, in 2007.

He is currently an Associate Professor with the Mechanical Engineering Department, Isfahan University of Technology, Isfahan, Iran.

Fanny Ficuciello (SM'17) is an Associate Professor with the University of Naples Federico II, Naples, Italy. She has authored more than 40 journal, conference papers, and book chapters. Her research interests include biomechanical design and bioaware control strategies for anthropomorphic hands, grasping, and manipulation; human–robot interaction; and surgical robotics.

She is an Associate Editor for the *Journal of Intelligent Service Robotics* and is currently a Principal Investigator of the MUSHA project (Multifunctional Smart Hands).

Bruno Siciliano (F'00) is a Professor of control and robotics, the Director of the Interdepartmental Center for Advanced Robotics in Surgery (ICAROS), and the Coordinator of PRISMA Lab, University of Naples Federico II, Naples, Italy. He has delivered more than 150 keynotes and has authored or coauthored more than 300 papers and 7 books. His book *Robotics* is among the most adopted academic texts worldwide, while his edited volume *Springer Handbook of Robotics* received the 2008 PROSE Award for Excellence in Physical Sciences and Mathematics. His research interests include robot manipulation, human–robot cooperation, and service robotics.

He was the recipient of several awards and he is also a Fellow of the ASME and IFAC. His group has been granted 20 European projects, including an Advanced Grant from the European Research Council. He was the President of IEEE Robotics and Automation Society and is currently a Board Director for the European Robotics Association.